P11R.14

OBSERVATIONS OF WINTER STORMS WITH 2-D VIDEO DISDROMETER AND POLARIMETRIC RADAR

Kyoko Ikeda[1], Edward A. Brandes[1], Guifu Zhang[2], and Steven A. Rutledge[3]
[1]*National Center for Atmospheric Research, Boulder, Colorado*
[2]*University of Oklahoma, Norman, Oklahoma*
[3]*Colorado State University, Fort Collins, Colorado*

1. Introduction

The Winter Icing and Storms Project 2004 (WISP04) was conducted from February to April 2004 in north central Colorado. Program objectives were to evaluate remote sensing techniques for icing detection and for quantifying winter precipitation in support of airport deicing operations. Measurements from a S-band dual-polarization radar and a two-dimensional video disdrometer are being used to develop radar-based algorithms to discriminate between rain and snow, quantify winter precipitation, and improve parameterization of winter precipitation in numerical forecast models. An ability to match radar-measured and disdrometer-based radar parameters is essential when developing algorithms for winter precipitation. Video disdrometers provide important information regarding hydrometeor size, shape, terminal velocity, and number concentration at high temporal resolution. As a first step in this project, we verify that the radar detects subtle changes in the character of winter precipitation.

Here radar reflectivity factor (reflectivity or Z_H, hereafter) and differential reflectivity (Z_{DR}) are calculated from disdrometer data collected on 5 March 2004, an event in which precipitation changed from rain to snow. The calculations are based on scattering amplitudes of raindrops and snow computed with the T-matrix method. The scattering matrix during the transition and snow phases was allowed to vary according to an empirical relation between particle size and bulk snow density developed from disdrometer observations. Reflectivity and differential reflectivity calculations based on disdrometer observations show good agreement with the radar measurements. The radar measurements of Z_H and Z_{DR} are then used to retrieve snow particle size distributions for comparison with the disdrometer observations. A case study from a precipitation event on 20 February 2004 will be also presented at the conference.

The dataset and a brief description of the disdrometer are given in section 2. Section 3 discusses the disdrometer calculations for reflectivity and differential reflectivity followed by a comparison of the estimates with the radar measurements in Section 4. Results from retrievals of particle size distributions are presented in section 5. A summary and concluding remarks are given in section 6.

* *Corresponding author address:* Kyoko Ikeda, National Center for Atmospheric Research, P.O. Box 3000, Boulder, CO 80307
E-mail: kyoko@ncar.ucar.edu

2. Data

The radar data were collected with NCAR's S-band dual-polarization radar located at Marshall, Colorado. Scan strategies included sector scans at 0.5 and 1.5° antenna elevation and range-height indicator (RHI) scans over a 2-D video disdrometer placed at a range of 19 km and an azimuth angle of 42° from the radar.

The disdrometer consists of two line-scan cameras providing front and side views of hydrometeors falling into the instrument. Each camera has a single line of 700 photo-detectors positioned opposite a light source. Hydrometeors falling through the 10 cm by 10 cm measuring area block the light source, shadowing some photo-detectors at a horizontal resolution of 0.15 mm. The number of blocked photo-detectors is recorded for each camera at a frequency of 51.2 kHz. Vertical resolution typically varies between 0.03 mm and 0.1 mm depending on particle fall speed. The sampling creates image projection slices of the hydrometeors.

Information provided on individual hydrometeors includes silhouette images, height and width information from each camera, and the particle terminal velocity. Particle terminal velocity is computed from the vertical distance between the two camera planes and the time the hydrometeor takes to break each plane. Raindrop axis ratio, canting angle, and horizontal velocity can also be obtained with the instrument. The disdrometer is equipped with temperature and wind sensors. A detailed description is found in Kruger and Krajewski (2002). Field notes from a crystal observer supplement the disdrometer data. Observations of crystal type, size, degree of riming, and amount of aggregation were made every 15 minutes.

3. Modeling considerations

Radar reflectivity (in $mm^6\ m^{-3}$) at horizontal (H) and vertical (V) polarization can be computed from

$$Z_{H,V} = \frac{4\lambda^4}{\pi^4 |K_w|^2} \sum_{i=1}^{M} N(D_i) \left| f_{H,V} \right|^2 \Delta D \qquad (1)$$

where λ is the radar wavelength, K_w is the dielectric factor of water, $N(D_i)$ is the size distribution for the *i*th size category having an equivalent diameter (mm) between D_i and $D_i + \Delta D$, *M* is the total number of size categories, and $|f_{H,V}|$ is the backscattering amplitude at horizontal and vertical polarization (see Zhang et al. 2001). Reflectivity is expressed in dBZ ($10\times\log_{10}Z_H$). In this study, the disdrometer data were quantitized into size categories of 0.2 mm over the range of 0.1-20.1 mm for snow and 0.1-8.1 mm for rain.

The differential reflectivity (Z_{DR} in dB) is defined as

$$Z_{DR} = 10 \times \log_{10}(Z_H / Z_V) . \qquad (2)$$

Z_{DR} is sensitive to particle bulk density, shape, and canting angle and can be interpreted as the reflectivity-weighted mean axis ratio of the illuminated hydrometeors. The Z_{DR} values were corrected for system bias (–0.08 dB). The bias was determined from radar data that was collected by rotating the antenna while pointing vertically in light rain. In theory, raindrops should produce a Z_{DR} value of 0 dB in the mean when viewed from below.

The scattering amplitude is computed with the T-matrix method (Barber and Yeh 1975). Input parameters include the dielectric constant, particle shape (e.g., axis ratio), and the temperature. For rain these parameters follow Zhang et al. (2001).

Properties of snow are complex. Aspect ratios and bulk densities continuously change throughout storm evolution making computations of the scattering amplitudes less straight forward. In this study, the particles were assumed to be oblate spheroids having a fixed axis ratio (vertical divided by horizontal) of 0.7 and with their major axis along the horizontal.

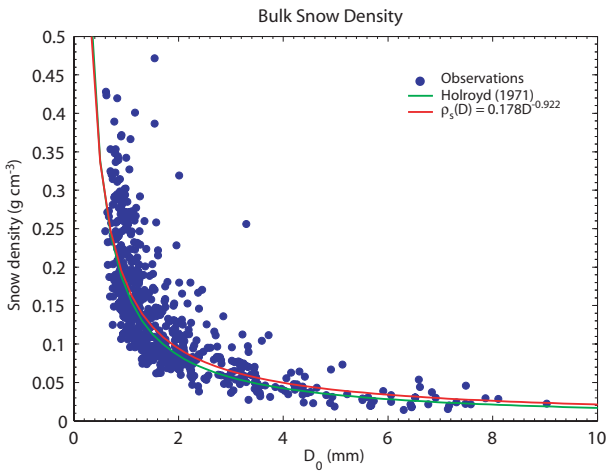

Figure 1: Relation between bulk snow density (ρ_s) and median equivolumetric diameter (D_0). Data points are from snow observations between February 2003 and April 2005. Each point represents an average quantity over a 5-minute interval. The red line is a power-law fit through the data points. An inverse relation (ρ_s = $0.170D^{-1}$) for unrimed snow aggregates from Holroyd (1971) is also shown.

The effective dielectric constant (Ishimaru 1991) was derived from an empirical relationship between snow bulk density and particle size based on disdrometer data collected at Marshall during winter seasons (Fig. 1). Snow bulk density was computed using 5-minute measurements of precipitation volume from the disdrometer and mass from onsite precipitation gauges. All instruments were located inside wind shields. Data points in Fig. 1 were from PSDs with total particle counts greater than 1000. Wind speeds were less than 2 m s^{-1}. The power-law relation between snow bulk density and median equivolumetric diameter is fitted though the data points (red line, Fig. 1). The dataset contains both rimed and unrimed snow. Nevertheless, the data closely follow the inverse relation between size and density found by Holroyd (1971) from ground-based observations of unrimed snowflakes. For this study, we use an effective dielectric constant based on the power-law relation derived from our disdrometer data. By using this relationship, the scattering amplitude allows for a variation in snow bulk density that is anticipated to occur with storm evolution. This approach is similar to that taken by Ryzhkov et al. (1998) who proposed a method to compute cloud ice water content using a relation between particle bulk density and radar cross sections or effective ice crystal diameter.

4. Observations: 5 March 2004

Precipitation on 5 March 2004 was dominated by an intense 500 mb trough across the western United States and an associated surface low pressure system over central Oklahoma. Low-level winds from the north and east-northeast behind the low pressure center created a favorable condition for upslope stratiform precipitation in the WISP04 domain. Above the upslope airmass (>5 km MSL), winds were mostly westerly or southwesterly, and the atmosphere was cloud-free. An abrupt decrease in surface temperature from 5.5°C to 0.5°C occurred over a 15-minute period at approximately 0100 UTC. The surface temperature changed only slightly afterward remaining between 0.5 and –0.5°C. The temperature at cloud top (4-5 km MSL) was generally between –13 and –18°C.

a. Precipitation

Most of the precipitation fell between 0000 and 0500 UTC. Table 1 summarizes the hydrometeor types noted by the crystal observer. Early precipitation was light rain (Period A). The surface layer moistened and cooled rapidly as the rain rate increased. A rain-to-snow transition (Period B) occurred with the temperature decrease at 0100 UTC. The field notes indicate ice pellets were mixed with raindrops. The smaller terminal velocities of ice pellets, compared with raindrops, are clearly depicted in the disdrometer data (Fig. 2). [Empirical relationships from previous

investigators are overlaid for reference.] A small number of large aggregates also existed at this time which caused an increase in the particle median volume diameter to 4.6 mm (Fig. 3). The mixed-phase precipitation period ended by 0120 UTC.

Later (0120-0145 UTC; Period C), observed precipitation consisted mostly of ice pellets and some small aggregates. Beginning at 0145 UTC (Period D), 1-3 mm plate-like crystals (plates and dendrites) became noticeable, and the number of large aggregates increased significantly. (Figs. 2 and 3, Period D).

Another change in precipitation occurred at approximately 0220 UTC. Small lump graupel and irregularly shaped snow pellets were mostly observed (Period E). The field notes indicate much less aggregation at this time. The terminal velocity appears to have a slightly stronger size-dependency compared with the previous stage (Fig. 2, Periods D and E). The median volume diameter decreased significantly between the period of heavy aggregation (Period D, D_0 = 6 mm) and the subsequent graupel/snow pellet Period E ($D_0 \leq 3$ mm). This change would correspond to an estimated bulk density increase of 0.05 g cm^{-3} (Fig. 1).

b. Comparison of the measured and calculated Z_H and Z_{DR}

Figure 4 shows time histories of measured and computed Z_H and Z_{DR}. The radar measurements were averaged over a 1-km radius circle centered at the disdrometer site. [The 0.5 and 1.5° elevation radar beams were 408 and 740 m above the disdrometer,

Table 1: Summary of hydrometeor observations taken at the disdrometer site. Particle types are listed from most to least common. Typical aggregate sizes (mm), percentage of total particles identified as aggregates, and degree of riming (none, light, moderate, heavy) are noted. Temperature ranges are from a sensor mounted on the disdrometer.

	Time (UTC)	Crystals	Aggregates	Temperature (°C)
A	0000-0100	Rain	—	5.5-7
B	0100-0120	Rain mixed with ice pellets	None	0.5-5.5
C	0120-0145	ice pellets	3-8 mm 30 % light	0.5
D	0145-0220	dendrites, plates, stellars	3-10 mm 40 % light to mod.	0.1
E	0220-0400	irregular snow, lump graupel	2-5 mm 5-20 % light	−0.5-0.1

respectively. These heights correspond to 1.93 and 2.26 km MSL.] The RHIs of Z_H and Z_{DR} were uniform in the horizontal; thus, the comparisons do not take in account particle trajectories. Figure 5 displays the time evolution of Z_H and Z_{DR} profiles at the disdrometer site. The Z_H retrievals with the disdrometer data in Period A are slightly less than the radar measurements. The Z_H cross section in the early rain stage shows an elevated layer of maximum reflectivity at ~3 km (Fig. 5). Evaporation at low levels may account for the offset between the estimated and measured values. When Z_H is computed assuming that all particles are snow in the rain period (Period A), the retrievals are significantly less than the measurements, reflecting the dependency of Z_H on the hydrometeor dielectric constant.

Agreement between the measured and computed Z_H are excellent during the snow period (after 0100 UTC). Well-matched retrievals in Period B, when using the snow scattering amplitude, come from the fact

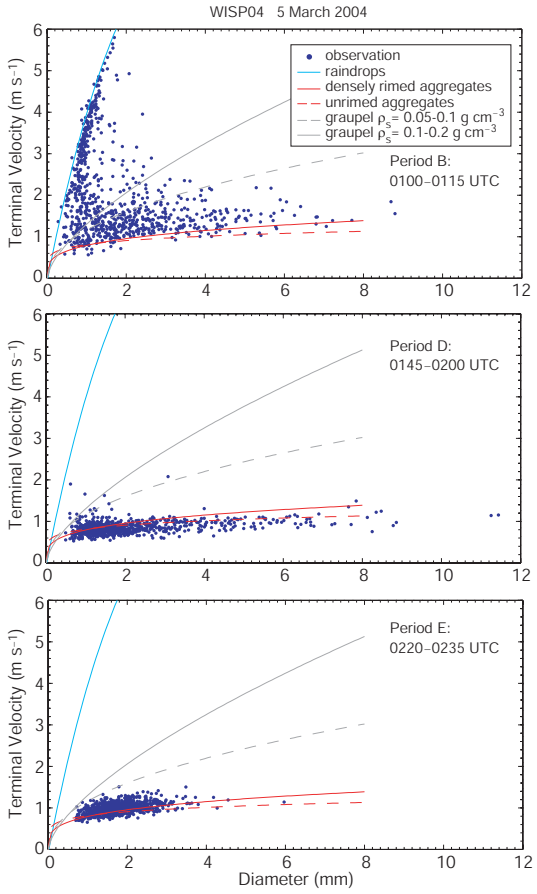

Figure 2: One-second averages of particle terminal velocity versus diameter for time segments in Period B (top), Period D (middle), and Period E (bottom). Hydrometeor observations during these time periods are indicated in Table 1. The terminal velocity relation for rain is from Brandes et al. (2002). The relations for graupel and snow aggregates are from Locatelli and Hobbs (1974).

that return signals from large, low density aggregates dominate over the returns from the smaller raindrops and ice pellets. An overall reduction in the particle size and an associated decrease in snowfall rate (Period D and Period E) coincides with a Z_H reduction of 10 dBZ or more throughout the cloud (Figs. 4 and 5).

Similarly, Z_{DR} calculations and measurements for the respective rain and snow phases show good agreement (Fig. 4). As with Z_H, Z_{DR} retrievals based on raindrop scattering amplitudes exceed the measurements during the rain-snow transition period. Correspondence for the snow period is attributable in large part to accounting for particle density changes. Small Z_{DR} is associated with low density aggregates in Period B through Period D. The measured and computed Z_{DR} values slightly increased when the number of aggregates significantly decreased and small graupel and snow pellets with higher density became dominant (Period E). This calculated Z_{DR} increase was not observed if the bulk density was fixed at a constant value of 0.05 g cm^{-3}.

Changes in precipitation microphysics can be inferred from Fig. 5. An overall decrease in Z_{DR} and increase in Z_H toward ground in Period B through Period D indicate that aggregation was taking place in the lower half of the cloud layer (below 3-3.5 km MSL, Fig. 5). Z_{DR} greater than 0.5 dB in the upper half of the cloud between 0130 and 0245 UTC suggests that these particles were more pristine. The temperature at cloud top was at approximately –13°C; thus the presence of plates and dendritic ice crystals is plausible (Magono and Lee 1966). Later, Z_{DR} increases and Z_H decreases in the lower half of the cloud layer (see for example below 3 km MSL after 0200 UTC) consistent with an increase in bulk density as detected by the disdrometer. Perhaps, the ice crystals originating at higher levels between 0130 and 0245 UTC arrived at the surface as graupel and heavily rimed ice crystals. A general decrease in Z_{DR} from 0.3 to 0.1 dB between the 1.5 and 0.5° elevation scans (Fig. 4) can be interpreted as evidence that particles were more oblate at higher elevations and that riming was taking place between the two scan levels causing the particles to become less oblate in the mean as they fell.

5. Retrievals of snow particle size distributions

Measurements of Z_H and Z_{DR} have been used previously to infer raindrop size distributions. Here, the retrieval procedure of Zhang et al. (2001) is applied to the data from Periods B-E. The retrievals are based on the definitions of Z_H and Z_{DR} expressed in terms of the Gamma PSD parameters [concentration parameter (N_0), shape factor (μ), and slope (Λ)], particle backscattering amplitudes, and an empirical relation between μ and Λ. The relation between μ and Λ was derived from the disdrometer observations in Fig. 1. The governing PSD parameters were obtained from the 2nd, 4th, and 6th moments of PSDs. For this dataset, μ and Λ are related by,

$$\mu = -0.004992\Lambda^2 + 0.7982\Lambda - 0.6658 \qquad (3)\,.$$

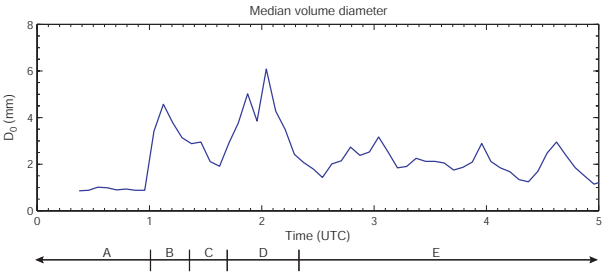

Figure 3: Changes in D_0 with time from 5-minute PSDs. Periods A-E are marked at the bottom.

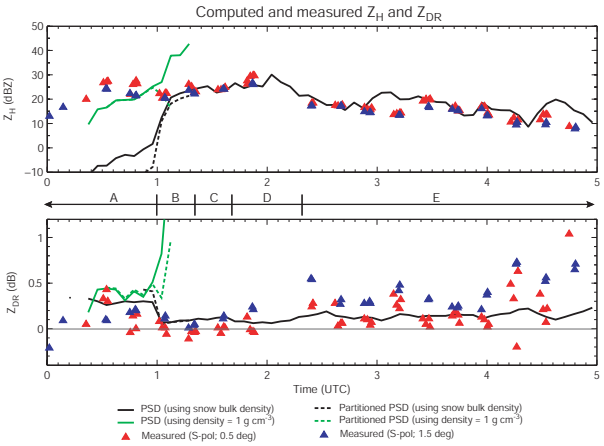

Figure 4: Time histories of measured and disdrometer-based estimates of Z_H (top) and Z_{DR} (bottom). Solid lines are the disdrometer-based estimates of Z_H and Z_{DR} based on 5-min PSDs assuming all particles are either snow (black) or rain (green). Dotted lines during the mixed-phased precipitation represent raindrops or snow particle contributions to the measurements. The disdrometer measurements of particle terminal velocities were used to partition data into raindrop and snow particle categories (e.g., Fig. 2, top frame).

Figure 6 compares the 3rd moments and total particle concentration (N_T) deduced from radar measurements and disdrometer observations. The 3rd moments, related to particle volume, match well between the two datasets. Total concentrations for Periods B and C are consistent with the observations. However, the correlation is poor between the observations and retrievals particularly for N_T from the 0.5° elevation scans after 0220 UTC (Period E) when smaller and denser particles become dominant. Discrepancies may arise partly from the fact that the bulk density rapidly changes toward smaller particle sizes (Fig. 1), the small dynamic range of Z_{DR} for snow, and because the zero-order moment of the PSDs is retrieved from higher moments. Additionally, the large negative bias is due to weak Z_H allowing ground targets to dominate and affect the Z_{DR} measurements. This is

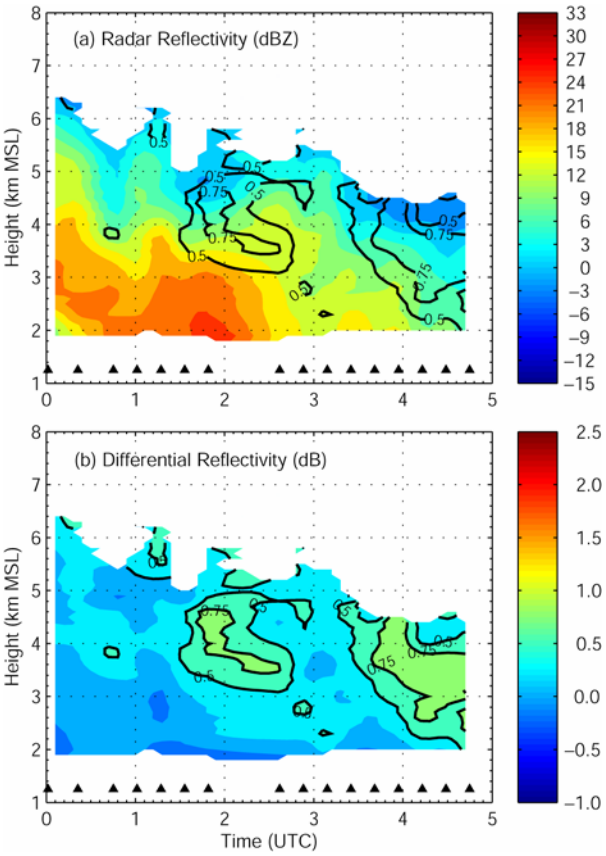

Figure 5: Height-time cross sections of (a) Z_H and (b) Z_{DR} at the disdrometer site based on RHI scans. Measurements were averaged over five azimuthal degrees and 2-km along-radial distances centered at the disdrometer site. Black contours show Z_{DR} of 0.5 and 0.75 dB.

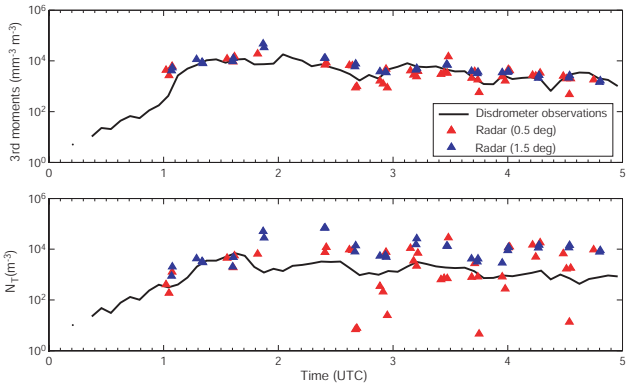

Figure 6: Time histories of the 3rd moments of particle size distributions and total particle concentrations. Solid lines are from disdrometer data and red (blue) triangles are the retrievals from the radar measurements of Z_H and Z_{DR} at 0.5 and 1.5° elevation angels, respectively.

clearly indicated by an increase in scatters in the N_T retrievals from the 0.5° scans.

Sensitivity of the retrieval procedure to ρ_s-D (i.e., scattering amplitudes) and Λ-μ relations were examined through simple sensitivity tests. The results show that an increase in bulk density by 0.02 g cm^{-3} can change the retrievals of the 3rd moments by nearly 50% and the total concentration by 60%. Similar retrieval sensitivity is expected for variations of particle axis ratios as they are also related to the scattering behavior of ice/snow particles.

The changes in the retrievals were less sensitive to variations in the Λ-μ relation. The improvement was most significant for N_T when the distribution was broadened and shifted to larger particle sizes. The root-mean-square error (RMSE) was reduced by 14% to 10.75x10^4 m^{-3}. On the other hand, making the PSDs narrower increased the RMSE by 30.4% to 16.43x10^4 m^{-3}. The changes were less noticeable for the 3rd moments. Test results suggest that the current retrieval procedure produces too many small, dense particles. Additionally, the results indicate that the technique is more sensitive to the choice of ρ_s-D relation than the Λ-μ relation.

6. Summary and concluding remarks

Radar reflectivity and differential reflectivity were computed from disdrometer data and were compared to radar measurements. The scattering amplitudes for snow particles were derived by exploiting an empirical relationship between particle size and snow bulk density. Overall, the comparisons showed good agreement. Large positive biases in the Z_H and Z_{DR} retrievals during the rain-snow transition period when applying the scattering amplitudes for raindrops disclose the importance of assuming the correct dominant hydrometeor type. The retrievals during the snow period mirrored the changes in hydrometeor habits. Aggregates were associated with small Z_{DR} and large Z_H as expected. An increase in bulk density, as the number of aggregates decreased and that of compact graupel increased, was reflected by a general increase in Z_{DR} and decrease in Z_H throughout the cloud layer. In this case, the use of the size-density relation was important in achieving good agreement between the computed values and measurements.

Reproduction of radar parameters with disdrometer observations is an important initial step in the development of radar-based algorithms for winter precipitation. Well-matched retrievals provide a foundation for reconstructing particle size distributions. Such a capability is required for improving microphysical parameterizations in numerical forecast models and quantifying winter precipitation from radar measurements.

The PSD retrieval procedure based on the measurements of Z_H and Z_{DR} produced an overall agreement in snow particle volume while the total particle concentration was generally overestimated. Results showed that the procedure is sensitive to the empirical relations between the snow bulk density and

particle size. This is in part due to the small dynamic range of Z_{DR} for snow while bulk density rapidly increases for particle sizes <2.5 mm. The retrievals were less sensitive to variations in the relation between slope and shape parameters.

The study of winter precipitation using disdrometer and radar is ongoing. In order to develop radar-based algorithm, examination of more datasets are in order. A field program is being planned to collect additional winter precipitation datasets with a polarimetric radar and 2-D video disdrometer.

Acknowledgement: This research is in response and funding by the Federal Aviation Administration (FAA). The views expressed are those of the authors and do not necessarily represent the official policy or position of the U.S. government. The authors are grateful for Dr. Michael Schoenhuber of the Joanneum Research for his thorough technical advice for the disdrometer operations.

References

Barber, P., and C. Yen, 1975: Scattering of electromagnetic waves by arbitrarily shaped dielectric bodies. *App. Optics*, **14**, 2864-2872.

Brandes, E. A., G. Zhang, and J. Vivekanandan, 2002: Experiments in rainfall estimation with a polarimetric radar in a subtropical environment. *J. Appl. Meteor.*, **41**, 674-685.

Holroyd, III, E. W., 1971: The meso- and microscale structure of Great Lakes snowstorm bands: A synthesis of ground measurements, radar data, and satellite observations. Ph.D. dissertation, State University of New York at Albany, 148 pp.

Ishimaru, A., 1991: *Electromagnetic Wave Propagation, Radiation, and Scattering*. Prentice Hall, 637 pp.

Kruger, A., and W. F. Krajewski, 2002: Two-dimensional video disdrometer: A description. *J. Atmos. Oceanic Technol.*, **19**, 602-616.

Locatelli, J. D., and P. V. Hobbs, 1974: Fall speeds and masses of solid precipitation particles. *J Geopys. Res.*, 79, 2185-2197.

Magono, C., and C. W. Lee, 1966: Meteorological classification of natural snow crystals. *J. Fac. Sci. Hokkaido Univ. Ser. VII*, **2**, 321-362.

Ryzhkov, A. V., D. S. Zrnić, and B. A. Gordon, 1998: Polarimetric method for ice water content determination. *J. Appl. Meteor.*, **37**, 125-134.

Zhang, G., J. Vivekanandan, and E. Brandes, 2001: A method for estimating rain rate and drop size distribution from polarimetric radar measurements. *IEEE Trans. Geosci. Remote Sens.*, **39**, 830-841.